Available online at www.sciencedirect.com
ScienceDirect
Trans. Nonferrous Met. Soc. China 31(2021) 3719−3738
Transactions of Nonferrous Metals Society of China
www.tnmsc.cn

Wear and corrosion behavior of clay containing coating on AM 50 magnesium alloy produced by aluminate-based plasma electrolytic oxidation

Farideh DAVOODI[1], Masoud ATAPOUR[1,2], Carsten BLAWERT[2], Mikhail ZHELUDKEVICH[2,3]

1. Department of Materials Engineering, Isfahan University of Technology, Isfahan 84156-83111, Iran;
2. MagIC−Magnesium Innovation Centre, Institute of Materials Research,
Helmholtz Zentrum Geesthacht, Max-Plank-Str. 1, 21502 Geesthacht, Germany;
3. Faculty of Engineering, University of Kiel, Kaiserstrasse 2, 24143 Kiel, Germany

Received 30 December 2020; accepted 5 August 2021

Abstract: This study aims to examine the effect of clay micro particles addition on the microstructure, wear and corrosion behavior of PEO coatings on AM 50 magnesium alloy. PEO coatings were prepared using an aluminate-based electrolyte with and without the presence of 5 g/L clay particles. The structure and composition of the coatings were evaluated using SEM, EDS and XRD. The wear investigations were conducted using a ball-on-disk tribometer at 2, 5 and 10 N loads. The corrosion behavior of the coatings was examined using polarization and EIS tests in 0.5 wt.% NaCl. The results revealed that the addition of clay particles deteriorated the wear resistance of the coatings under the loads of 5 and 10 N. The SEM examinations of the worn surfaces indicated that a combination of adhesive and abrasive wear mechanisms was activated for the coating with clay particles. The poor wear performance of the clay-incorporated coating was related to its lower adhesion strength and higher roughness. The potentiodynamic polarization examinations revealed that the addition of clay particles slightly decreased the corrosion rate of the coatings. Corrosion resistance of the clay-containing coating was attributed to its compactness, as indicated by the results of EIS tests.
Key words: wear; corrosion; clay particles; plasma electrolytic oxidation; Mg alloys

1 Introduction

Magnesium and its alloys are promising materials for use in many applications due to their unique properties such as high specific strength, high dimensional stability and good machining and recycling ability [1−4]. The application of Mg alloys in various industries including automobile, aerospace and communications can bring great benefits of weight reduction and lower cost [5−7]. However, the applications of Mg alloys is often restricted by their poor corrosion and wear properties [1,8−11]. To cope with these disadvantages, different surface treatments have been established for protection of Mg alloys. The latest important advances in different conversion, deposition, mechanical and functional coatings applied for Mg alloys have been recently reviewed in Refs. [12,13]. In this respect, plasma electrolytic oxidation (PEO) has gained great technical interest for Mg alloys in recent years [14,15]. PEO is a relatively new surface treatment, and it is a modified version of the traditional anodic oxidation [16]. PEO is a rather inexpensive and environmentally friendly method with many advantages such as less pre-treatment process and easier operation [15]. In this surface treatment, an

Corresponding author: Masoud ATAPOUR, E-mail: m.atapour@cc.iut.ac.ir
DOI: 10.1016/S1003-6326(21)65759-X

extremely adhesive oxide coating is formed on the surface due to occurrence of a plasma discharge and partial fusion of the oxide film [17]. The PEO coatings are able to significantly improve the wear and corrosion behavior of the Mg alloys.

In recent years, many studies have focused on the PEO coatings on Mg alloys. For instance, LI et al [18] reported that the addition of carbon spheres in the silicate electrolyte during PEO process improved the wear and corrosion resistance of the PEO coatings. CUI et al [19] fabricated a PEO/polymethyltrimethoxysilane (PMTMS) hybrid coating on AZ31 alloy and reported that the corrosion resistance of the coating was enhanced due to self-healing behavior of PMTMS. In another work by ZHANG et al [20], the corrosion behavior of the PEO coating was investigated in an electrolyte of phosphate buffer saline (PBS) containing bovine serum albumin (BSA). It was found that the adsorption of BSA improved the corrosion resistance of the PEO coating. According to LI et al [21,22], the corrosion resistance of the PEO coated AZ31 Mg alloy was improved by doping the antimony tin oxide or deposition of tantalum oxide nanofilm on PEO coating.

PEO coatings have also been used in duplex treatments for improving the wear and corrosion resistance. For instance, it has been reported that the cold spray process with high hardness and a compact structure improved the corrosion resistance of AZ31 Mg alloy in Hank's solution [23]. Also, the cold spray process followed by PEO treatment enhanced the wear and corrosion resistance of Mg alloys [24,25].

It is well known that the PEO treatment of Mg can be carried out in silicate, aluminate or polyphosphate-containing alkaline electrolytes [26]. Depending on the electrolyte and treatment parameters (current density, frequency and current type), the PEO coatings on Mg alloys are composed of amorphous and crystalline phases [27]. Many investigators have focused on exploring and/or optimizing the electrolyte composition and/or electrical parameters to improve the wear and corrosion of PEO coatings [28]. However, the presence of discharge channels and porosity is the main concern for such PEO coatings. The in-situ incorporation of nano/micro particles into the PEO coatings by adding the particles into the solution appears to be a promising direction of PEO process development in recent years [2,29−31]. The electrophoretic deposition, melting and plasma thermo-chemical reactions are the main phenomena controlling the incorporation of particles into the coatings [32]. Different aspects of the particles addition in PEO electrolytes were recently presented and reviewed by FATTAH-ALHOSSEINI et al [33].

It has been reported that the addition of low melting point particles in the electrolyte of PEO treatment can be beneficial in filling the pores by occurrence of the melt re-flow and liquid phase sintering [34]. In this regard, low-melting-point clay particles (<1200 °C) have been used in some works to fill the discharge channel. First successful incorporation of clay particles into the PEO coatings on magnesium alloy has been reported by BLAWERT et al [34] using phosphate and silicate based electrolytes. They have demonstrated that the PEO coating with clay produced in phosphate electrolyte exhibited a more compact structure compared to coatings produced in silicate based electrolyte. In the work by RAPHEAL et al [32], the influence of current densities on the microstructure and corrosion of phosphate-based PEO coatings with clay addition was investigated and it was found that higher current densities (120 mA/cm^2) led to the formation of a more defective barrier layer and high porosity in the outer porous layer. LU et al [30] focused on the corrosion behavior of PEO coatings produced in phosphate electrolyte containing montmorillonite clay particles. They reported that the clay particles are able to incorporate into the PEO coating in a reactive manner. In a newer study by this group [29], the corrosion and wear resistance of the PEO coatings prepared in phosphate-based electrolyte with and without addition of particles with different melting points including clay, SiO_2, Si_3Ni_4 and SiC micro-sized particles were investigated. They have reported that the melting point of the particles is a key factor influencing the incorporation mechanism under the same PEO parameters. Their results showed that the addition of clay can improve the corrosion and wear behavior of the coatings due to its reactive incorporation. However, more details on the wear behavior of coatings (such as wear of counterpart) were not reported.

Dry sliding wear behavior of PEO-coated

magnesium alloys, is important to consider in terms of widespread use of magnesium alloys in the automotive industry applications (including automotive brakes, guide bars, bearing plates, seat supports, and engine components (piston and cylinder brakes)). It needs to note that magnesium alloys show very poor tribological behavior in the absence of lubricants [35]. PEO treatment is able to improve the wear resistance of Mg alloys by formation of a thick and hard ceramic-like oxide coating [36].

Although considerable investigations have been carried out on the wear of PEO coatings reinforced by particles with a relatively high melting point, the studies on the wear behavior of the PEO coatings incorporated with low melting particles like clay are still in the infancy stage. In this study, the microstructure, wear behavior and corrosion performance of the clay incorporated PEO coatings produced in an aluminate-based electrolyte were investigated systematically. To our knowledge, no one has studied the wear and corrosion behavior of the aluminate-based PEO coatings with clay particles.

2 Experimental

2.1 Materials

Square plates with dimensions of 25 mm × 25 mm × 4 mm were machined from the AM50 magnesium alloy (4.74 wt.% Al, 0.383 wt.% Mn, 0.063 wt.% Si, 0.065 wt.% Zn, 0.002 wt.% Fe, 0.002 wt.% Cu and balance Mg). Before PEO treatment, the specimens were ground with emery papers up to 1200 grit, then cleaned with ethanol and finally dried in compressed air flow at room temperature.

2.2 PEO treatment

PEO treatment was conducted in an aluminate-containing electrolyte ($NaAlO_2$ (12 g/L), Na_3PO_4 (8 g/L) and KOH (1 g/L) using a pulsed DC power source (Elektro-automatik EA-PS 8720-15 720 V) at a constant current density of 65 mA/cm^2 for the treatment time of 10 min. The clay particles with the average size of 12 μm (Rockwood Nanofil® 116, natural montmorillonite (about 100% bentonite) were used to produce PEO coatings containing clay. The pulse ratio was t_{on}:t_{off} = 2 ms:18 ms. The specimens and a stainless steel tube were used as the anode and cathode, respectively. According to the experiences of our group and our previous papers [30,32], 5 g/L clay particles were dispersed into the PEO electrolyte. The corresponding coatings were named PEO (without clay particles) and PEO-Clay (with clay particles), respectively. Table 1 summarizes the composition, conductivity and pH of the electrolytes used in this work.

Table 1 Specification of PEO electrolytes used to coat samples

Sample	Composition/(g·L^{-1})			
	KOH	$NaAlO_2$	Na_3PO_4	Clay
PEO	1	12	8	0
PEO-Clay	1	12	8	5
Sample	Conductivity/(mS·cm^{-1})			pH
PEO	23.7			12.5
PEO-Clay	23.2			12.6

A cooling system was utilized to maintain the temperature of the electrolyte bath constant at (20±2) °C. The conductivity and pH value of the electrolytes were measured using a Mettler Toledo Inlab 730 probe and a Metrohm 691 pH meter, respectively. Also, a bubble generator was used to keep the particles suspended during the treatment.

2.3 Characterization

The surface morphology and cross section of each coating were identified using a Tescan Vega3 scanning electron microscope (SEM) equipped with energy dispersive X-ray spectroscopy (EDS). In order to observe the morphology of the coatings in cross section view, the coated samples were embedded into resin, polished successively up to 2500 grit emery sheets and finally polished using the diamond paste (1 μm). X-ray diffraction (XRD) technique (GIXRD, D8 Advanced Bruker AXS using a Cu K_α source wavelength of 1.54056 Å in the range from 10° to 80°) was used to determine the phase composition. The surface roughness of the coatings was determined using a Hommel profilometer (HOMMEL TESTER T1000).

2.4 Bonding strength

Bonding strength of the coatings was measured using a Hounsfield H25KS universal

testing machine, according to ASTMC-633 [37]. Parallel aligned cylinders were glued to the coated and back sides of the coupons by 3M Scotch Weld-2214 epoxy resin. The load required to detach the coating from the substrate with tested contact area (3.14×12.5^2 mm^2) was measured. The coating adhesion strength was obtained by dividing the load by the surface area. Measurements were repeated three times and the average of bonding strength was calculated.

2.5 Wear tests

Dry sliding wear behavior of the PEO coatings was examined with a ball-on-disc tribometer (TRIBO technic−France). An AISI 52100 steel ball with 6 mm in diameter was used as the static sliding counter body. All the studies were carried out in air at a temperature of (25±2) °C and a relative humidity of 30%. The wear tests were performed under 2, 5 and 10 N loads with oscillating amplitude of 10 mm and at a sliding velocity of 5 mm/s for 60 min. The wear tracks and the worn ball surfaces were examined using SEM and EDS. All tests were performed at least three times to ensure reproducibility.

2.6 Corrosion tests

The corrosion performance of the coated samples was studied using a computer controlled potentiostat system (Gamry Interface 1000) in 0.5 wt.% NaCl at room temperature. A three-electrode electrochemical cell system was used for potentiodynamic polarization tests. Saturated Ag/AgCl electrode, platinum mesh and coated specimens were used as reference, counter and working electrodes, respectively. The tested surfaces were 0.5 cm^2. The potential of working electrode continuously increased from −250 mV to +500 mV vs. Ag/AgCl with respect to the open circuit potential (OCP) at a scan rate of 0.5 mV/s in potentiodynamic polarization tests. Tafel extrapolation method was used for extracting the corrosion parameters.

EIS measurements were conducted at room temperature with the 0.01 V amplitude of sinusoidal voltage after 1 h immersion in 0.5 wt.% NaCl, in the frequency range from 100 kHz to 10 mHz. The corrosion tests were repeated at least three times for each sample.

3 Results and discussion

3.1 Microstructure

The surface morphologies of PEO and PEO-Clay coatings are shown in Fig. 1 and Fig. 2, respectively. As can be seen, the surface of both coatings exhibited the characteristic features of the PEO coatings consisting of pores and cracks within the coating. The open pores in PEO coatings were formed due to eruption and subsequent rapid solidification of the coating materials. The pore size and coating roughness were strongly affected by addition of clay particles. Without clay particles, the coating was smoother which was proven by roughness (R_a) values of (1.4±0.1) μm and (2.56±0.1) μm for the PEO and PEO-Clay coatings, respectively. This trend is in accordance with the previous works on the clay-incorporated PEO coatings [34]. In agreement with our previous works [29,34], the addition of clay particles decreased the size and the number of open pores. This behavior can be related to the low melting point of clay particles which can reduce the viscosity of the melt and increase the melt volume. The addition of clay particles led to the formation of some bigger closed pores [34]. It can be deduced from Fig. 2 that the size of the filled pores is larger than the size of open pores. It seems that there was not the possibility of closing the pores by liquid melt before solidification of the formed open pores [34]. It has been demonstrated that a fully reactive incorporation of clay particles occurred to improve the PEO coatings [38]. Also, the formation of micro-cracks in the coatings can be attributed to the presence of thermal stresses and the phase transformations (in the oxide films) during treatment [39].

Surface compositions of PEO and PEO-Clay coatings were investigated using EDS examinations and the results are presented in Table 2. These results confirmed the presence of O, Na, Mg, Al and P on the surface of both coatings. The presence of Si in the PEO-Clay coating was due to successful incorporation of clay particles. It should be noted that clay particles were the only source of Si.

In order to obtain more information on the surface composition of the coated specimens, the EDS elemental maps of PEO and PEO-Clay coatings were achieved and presented in Fig. 1(c−g)

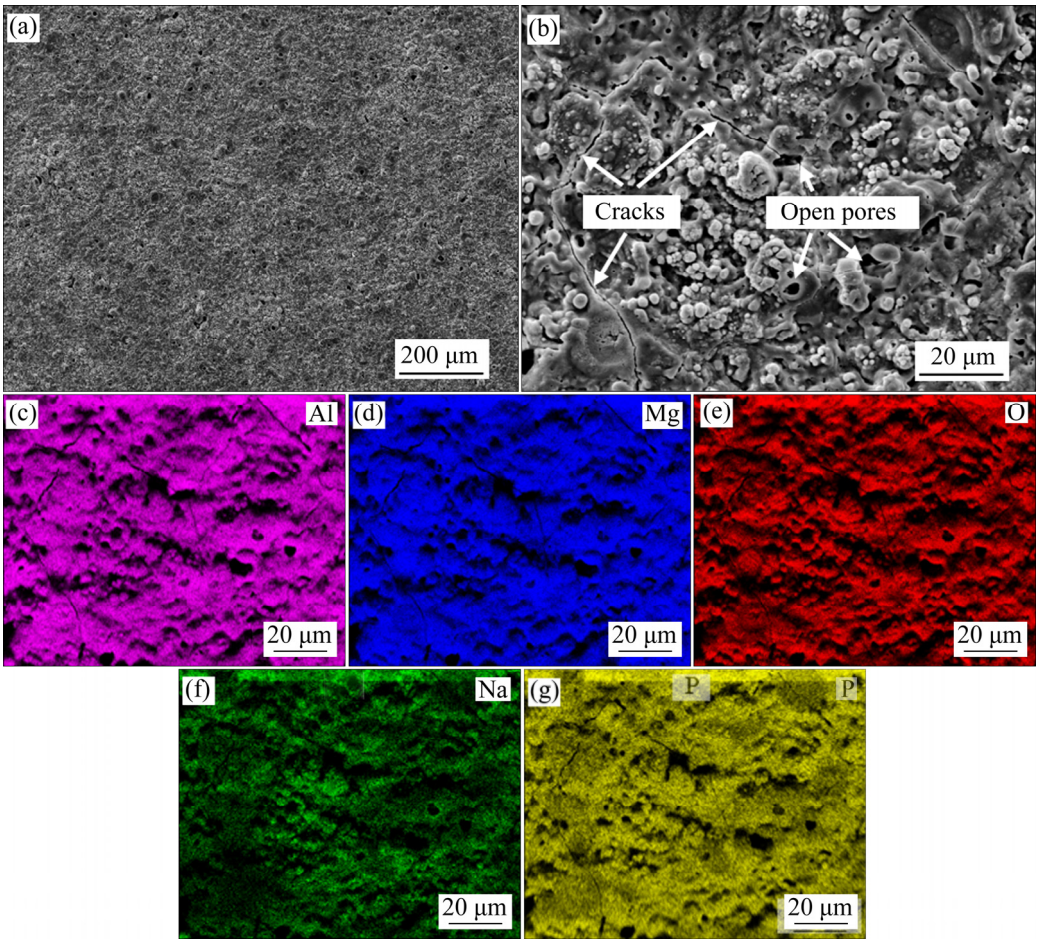

Fig. 1 Surface morphology (a, b) and EDX maps (c−g) of PEO coating

Table 2 EDS results of top surface of coatings (wt.%)

Coating	O	Na	Mg	Al	P	Si
PEO	33	3	24	27	13	0
PEO-Clay	34	2	19	24	13	8

and Fig. 2(c−h), respectively. A uniform distribution of elements was observed across the coatings. A similar result has been observed in the work by TOULABIFARD et al [40] for the PEO coating obtained in the aluminate electrolyte. It needs to note that the low concentration of Na on the top surfaces can be due to the low mass fraction of this element in the electrolyte. However, except in the open pores, both coatings were rich in other elements.

Based on the cross section of the PEO coatings (Figs. 3(a, g)), it can be deduced that the addition of clay particles did not have a significant effect on the coating thickness. In other words, the growth rate of the coatings was similar in the presence and absence of the clay particles. Similar behavior was reported for other particles [14,41]. According to RAPHEAL et al [32], a uniform uptake of clay particles occurred across the cross section and also the clay particles might migrate through the interlinked pores into the interface of the coating/substrate. SAH et al [42] showed that a pore band was formed due to the penetration of the melted material into inner part of the PEO coating. It seems that the large discharge channels were not filled and this led to the formation of the pore bands [30]. As can be seen in Fig. 3, the pore bands were formed in both coatings but the volume of pore bands was increased in the coating with clay particles. BLAWERT et al [34] stated that the formation of thicker pore bands in the PEO-Clay coating was related to the formation of gas inclusions and higher plasma discharges during PEO-Clay treatment. In contrast, it seems that the pores and porosities in the outer layer of PEO coating were more than those formed in the PEO-Clay coating.

In order to identify more details of the particles distribution of the coatings, the EDS

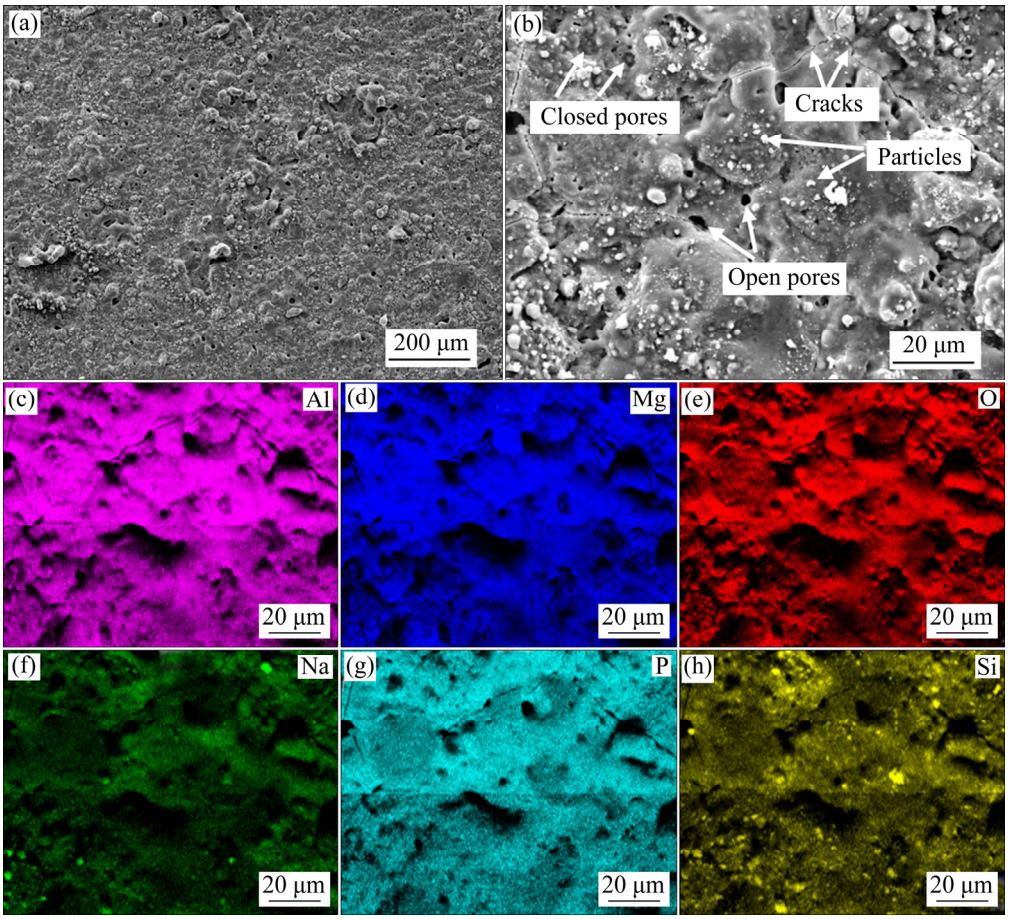

Fig. 2 Surface morphology (a, b) and EDX maps (c−h) of PEO-Clay coating

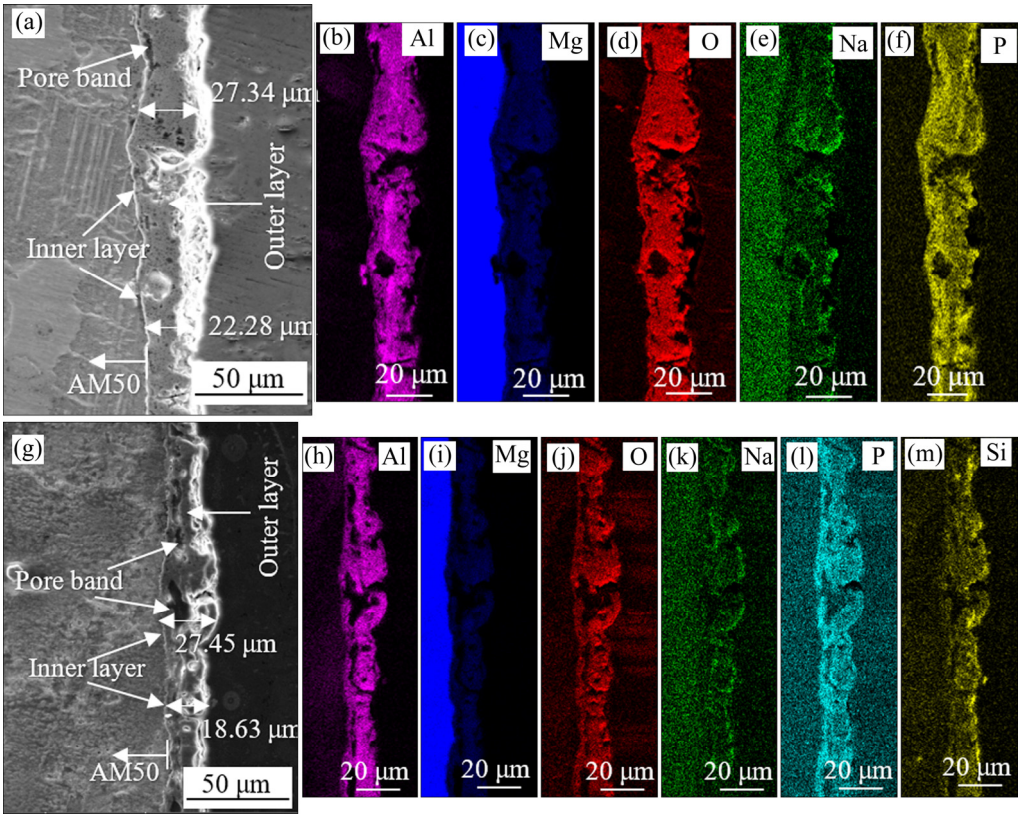

Fig. 3 Cross-section (a, g) and elemental maps (b−f, h−m) of PEO coating (a−f) and PEO-Clay coating (g−m)

mapping was conducted on the cross section. For both coatings, a uniform distribution of O, Mg, P, Na and Al elements was observed across the whole layer. For PEO-Clay coating, a homogenous Si layer was also formed across the cross section. It can be deduced that some particles were intact on the outer layer of the surface. In other words, there might be a different up-take mechanism for the incorporated clays on the outer layers. It needs to note that the clay particles with low melting point were melted easily by short-lived discharges and subsequently reacted with other components [43].

Figure 4 shows the phase composition of the prepared coatings. It can be seen that $MgAl_2O_4$ was the main crystalline phase of both coatings. This phase was formed due to the reaction of Al_2O_3 (from the electrolyte) and MgO (from the substrate) during sparking process at high temperature [43]. The appearance of the Mg peaks is related to the penetration of X-ray into the thin coatings. However, the intensity of $MgAl_2O_4$ peaks in the case of PEO-Clay coating was weaker compared to that observed for the particle-free coating. This means that the addition of clay particles decreased the crystallinity of the PEO coating. Thus, the PEO-Clay coating probably contained a mixture of the amorphous and crystalline phases. Due to the low amount of Si (Table 2) in the PEO-Clay oating, no clear amorphous peak was observed.

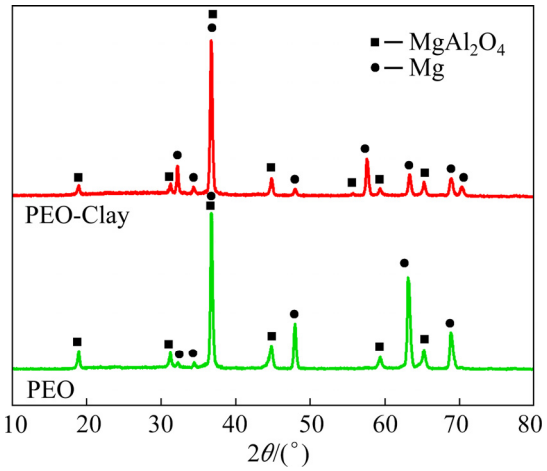

Fig. 4 XRD patterns of PEO and PEO-Clay coatings

3.2 Tensile adhesion test results

Figure 5 depicts the load–displacement curves obtained from the uniaxial tensile adhesion test. The adhesion strength of a coating is considered as one of the main mechanical aspects of this coating system. The applied load reaches the maximum as soon as the failures occur or the coating is broken. Due to the high level of the adhesion strength of both coatings, a cohesive debonding within the thickness of both coatings occurred. Cohesive strength of the PEO and PEO-Clay coatings were 11.40 and 9.32 MPa, respectively. Lower cohesive strength of PEO-Clay coating can be attributed to the agglomeration of the clay particles which triggered to the poor adhesion between the matrix and clay particles, as reported previously [44].

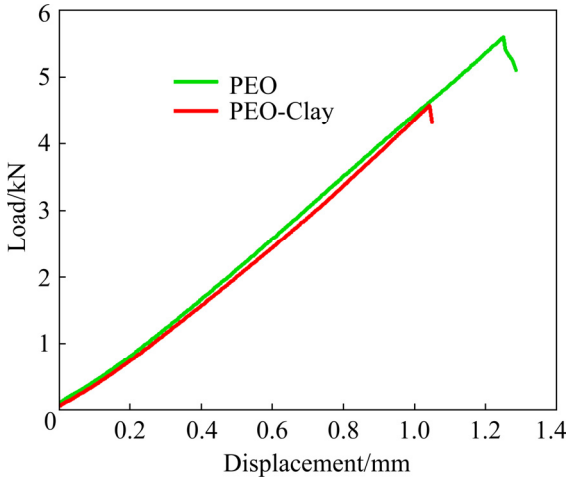

Fig. 5 Load−displacement curves of coated specimens

3.3 Wear assessment

The plots of friction coefficient against sliding distance for examinations at 2, 5 and 10 N loads for PEO and PEO-Clay coatings are illustrated in Fig. 6. It can be seen that the addition of clay particles significantly affected the wear behavior of the coatings. At 2 N, the PEO coating showed a steady-state friction coefficient of 0.47 after an initial 9 m of sliding. The periodic material transfer due to adhesive wear can be considered as the main source of the appearance of fluctuations leading to the formation of transfer layer and subsequent formation of wear debris by fracture of this transfer layer [45]. In comparison to PEO coating, the PEO-Clay coating exhibited a very similar friction coefficient at 2 N load and no drop in friction coefficient was observed. This means that the PEO and PEO-Clay coatings were both resistance against wear at 2 N load for 18 m wear evaluation. However, the steady-state friction coefficient value of PEO-Clay was a bit higher than that recorded for the PEO coating. This behavior can be related to the rougher surface of the PEO-Clay coating. Under

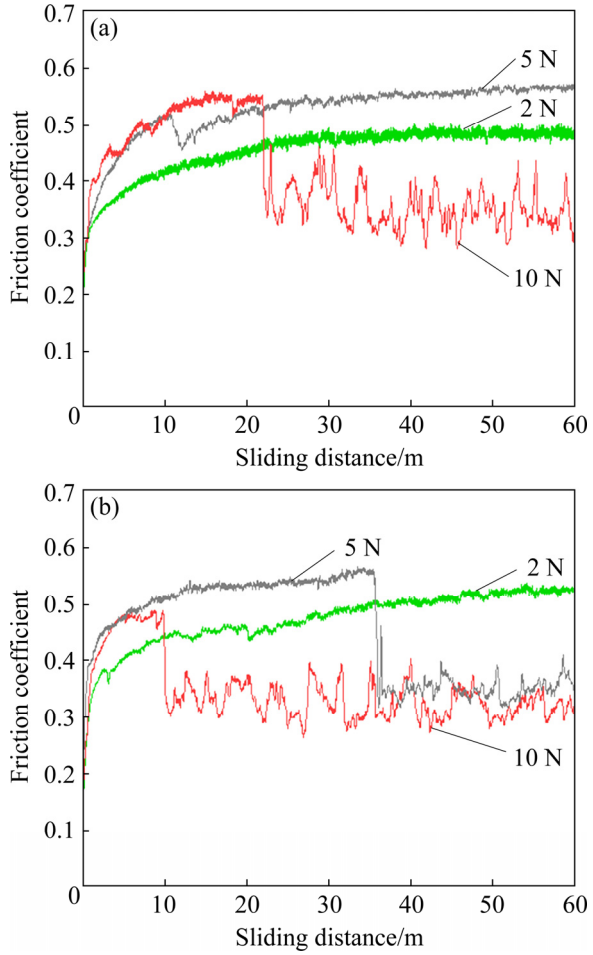

Fig. 6 Variation of friction coefficient for PEO (a) and PEO-Clay (b) coatings at 2, 5 and 10 N loads

5 N load, a distinctly different wear behavior was identified for the PEO and PEO-Clay coatings. When the PEO coating was resistant against wear, a sharp drop in friction coefficient was recorded after about 11 m of sliding for the PEO-Clay. Furthermore, the friction coefficient of both coatings was increased under 5 N when compared to that under 2 N. This increase can be attributed to enhancing the contact area between the specimen and steel ball by filling the cavities with the wear debris [46]. In the wear examinations under 10 N load, the friction coefficients were almost similar to those at 5 N load. However, a large drop in friction coefficient of both coatings was observed, which demonstrated the abrupt failure of the coatings at 10 N load. As shown in Fig. 6(b), the drop of the friction coefficient of the PEO-Clay coating occurred at shorter time (in less than 3 m of sliding) compared to that reached in the PEO coating. The friction coefficient of PEO-Clay coating dropped to around 0.35 after failure which corresponds to the untreated magnesium alloy (slide against steel ball contact) [14]. This means that the addition of clay particles deteriorated the wear behavior of the coating.

The wear rates of both coatings after wear examination at different loads were calculated and illustrated in Fig. 7. For all loads, a higher wear loss for the PEO-Clay was observed when compared to the PEO coating. Also, PEO-Clay coating revealed the highest wear rate of 2.84×10^{-4} $mm^3/(N\cdot m)$ after testing at 10 N load. It is obvious that the incorporation of clay particles could deteriorate the wear resistance of the coatings, specifically for the coatings under heavy load [8], leading to a higher penetration of counter face material [1]. The inferior wear resistance of the PEO-Clay can be attributed to a low adhesive strength, lower load bearing capacity [47] and stress concentration on surfaces [48].

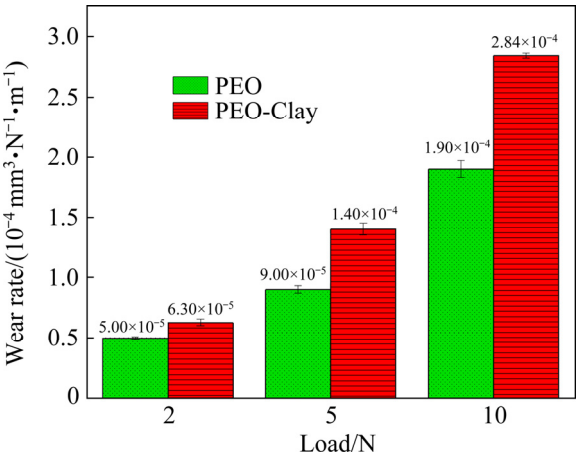

Fig. 7 Wear rates of PEO and PEO-Clay coatings

In order to obtain more details of the wear mechanisms, the wear tracks were investigated by scanning electron microscopy. As shown in Fig. 8, with the load further increasing to 10 N, the wear tracks become larger than those of the coating tested under lower load. Very similar worn surfaces with wear scars were observed for both PEO and PEO-Clay coatings at a load of 2 N. Both coatings were intact and the original coatings were observed without severe failure. In terms of the wear tracks under loads of 5 and 10 N, a distinct difference can be observed between the PEO and PEO-Clay coatings. The PEO coating was still intact at 5 N, while the PEO-Clay coating was found to undergo a more severe wear with large amounts of wear debris during the wear test. A higher magnification SEM

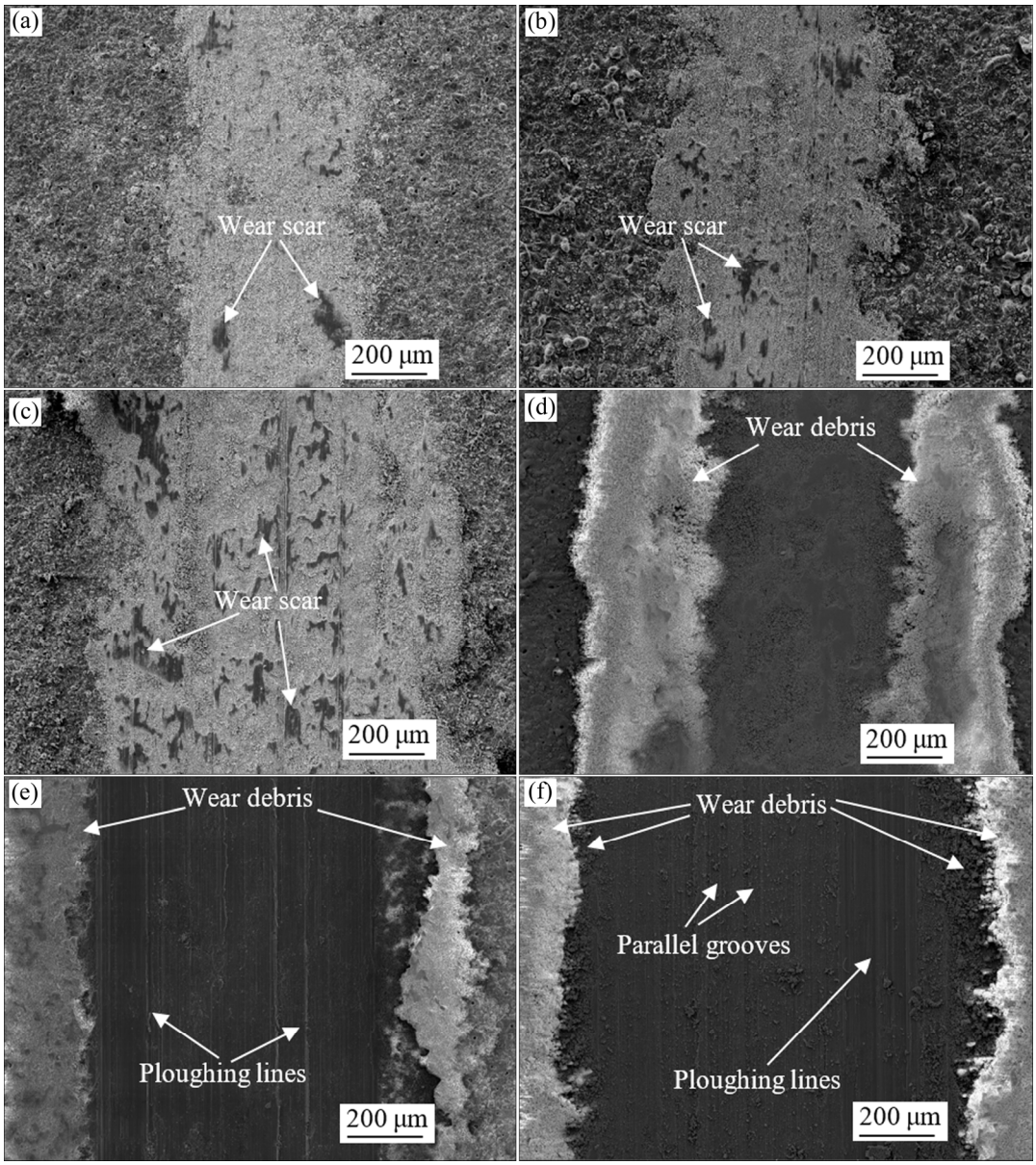

Fig. 8 Wear track morphologies (SEM images) of PEO (a, c, e) and PEO-Clay (b, d, f) coatings after sliding against steel ball under 2 N (a, b), 5 N (c, d) and 10 N (e, f) loads

micrograph of the worn surface of the PEO-Clay coating tested under 5 N load is illustrated in Fig. 9(a). In this case, many cracks could be seen in the wear track. High amount of Fe in the wear track of Fig. 9(a) (as displayed in EDS in Fig. 9(c)), can be attributed to the material transfer between the friction pairs [49]. The worn surfaces of the PEO and PEO-Clay coatings revealed that the coatings were completely removed during the wear examinations at 10 N load. However, the appearance of the wear tracks under 10 N load was different for the PEO and PEO-Clay coatings. It can be seen that the width and volume of the worn surface of PEO-Clay coating were larger than those of the PEO coating tested under 10 N load. The wear tracks were associated with parallel grooves or ploughing lines, which were identified as the main signs of abrasive wear occurring at 10 N. After the removal of coating, the bare metal surface experienced both abrasive and adhesive wear mechanisms [14]. Figures 9(b, d) show the higher magnification SEM micrograph of the worn surface of PEO-Clay coating tested at 10 N load and the point EDX analysis result of the box region in Fig. 9(b), respectively. As can be seen, granular wear debris was formed around the wear track. The dominant wear mechanism can be abrasive wear associated with three body mechanism action of

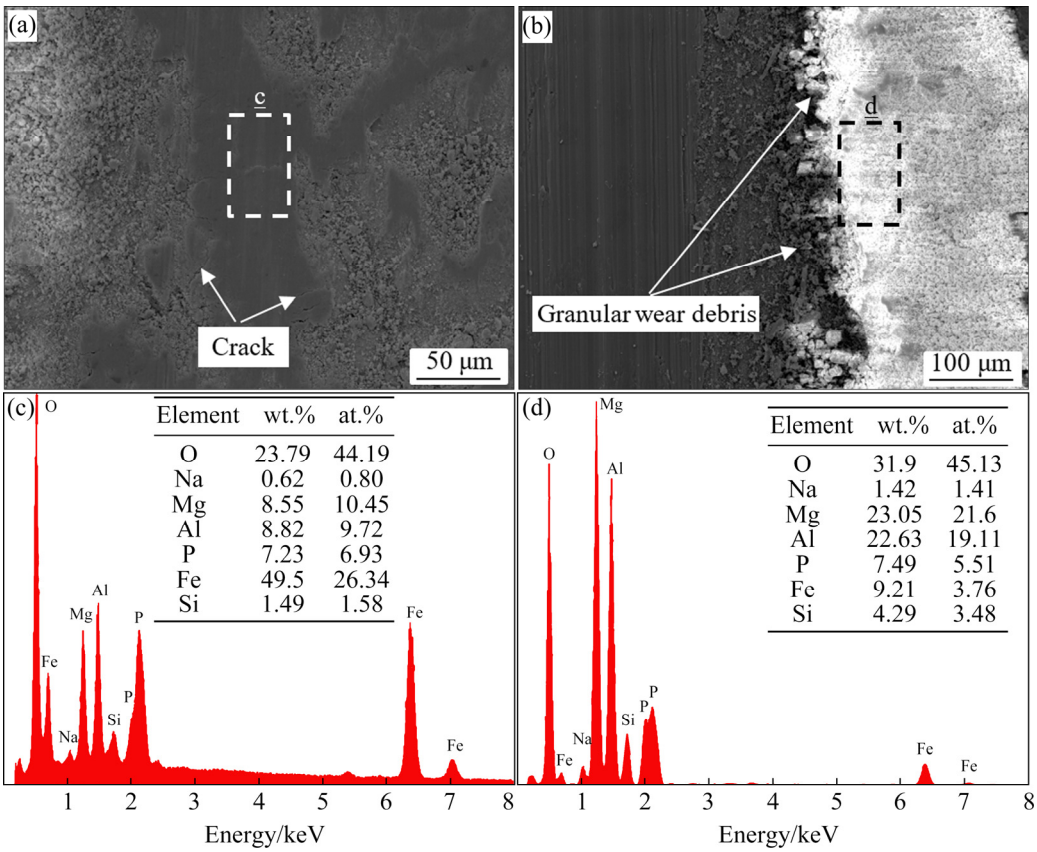

Fig. 9 SEM images (a, b) and corresponding EDS analysis results (c, d) of worn surfaces of PEO-Clay coating after sliding against steel ball under 5 N (a, c) and 10 N (b, d) loads

worn debris between coating and steel ball. The presence of O can be linked to the formation of magnesium oxide and iron oxide in the wear debris [50]. The results confirm that the porous nature of these coatings is detrimental to wear resistance [45].

According to the previous works on the PEO coatings with clay particles [51,52], the clay nanoparticles agglomeration and poor adhesion between the matrix and clay particles were reported as the main factors triggering abrasion damage in the coating with clay particles. Also, the particle size is a key factor influencing the wear behavior of the PEO coatings [53]. LU et al [29] reported that the addition of clay particles can improve the wear resistance of phosphate-based PEO coating. However, the use of clay micro particles (12 μm) in this work led to negative effect on the wear performance of the PEO coating. It seems that the removed particles from the PEO surfaces acted as a third body and consequently promoted additional abrasive load during the wear tests [53]. The higher roughness of the PEO-Clay coating was also an important factor in relation to poorer wear resistance of this coating. The effect of coating roughness on the wear properties has also been studied [14,40,54]. Moreover, the abrasive wear performance strongly depends on the ductility of the material and the fraction of the reinforcement in the composites [51,55]. SRINATH and GNANAMOORTHY [55] showed that the addition of the clay gives brittleness to a polymer clay nanocomposite and less ductility makes less wear resistance. In the present case, it seems that the addition of the clay decreases the ductility of the PEO coating. As the ductility reduces, the energy to rupture the coating also decreases and therewith increases the material removal from the surface. So, this causes the enhancement in the abrasive wear for PEO-Clay coating more than PEO coatings without clay particles especially at high loads.

Figure 10 exhibits the wear depth profiles of the PEO and PEO-Clay coatings examined under different loads. The results were consistent with friction coefficients and wear track morphologies. As can be seen in Fig. 10(a), it was difficult to

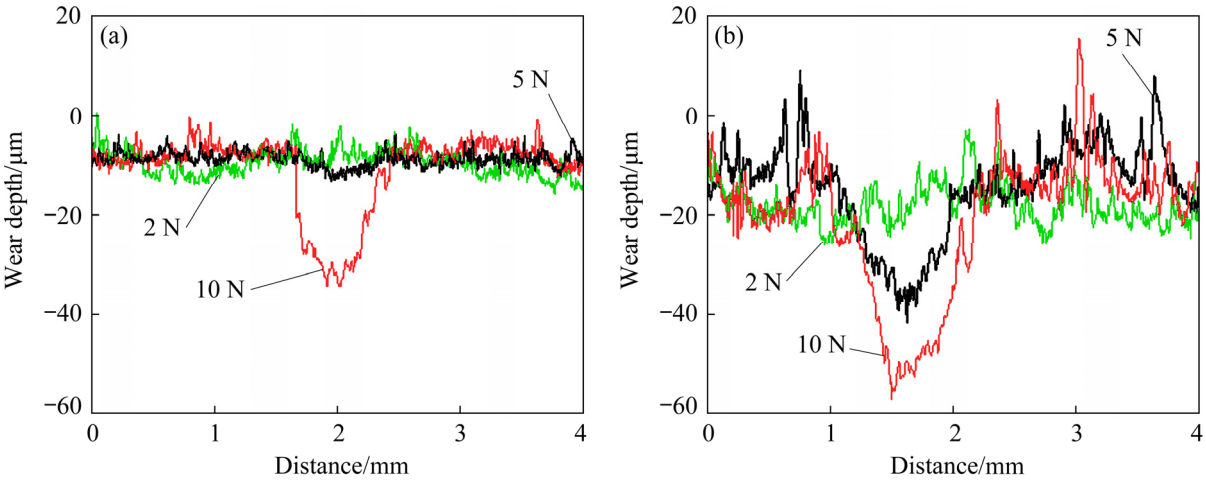

Fig. 10 Wear depth profile under different loads for PEO (a) and PEO-Clay (b) coatings

measure the depth in the wear track of PEO coatings at 2 and 5 N loads, while for 10 N load, the width and depth of the wear track were about 750 and 35 μm. For the wear depth of PEO-Clay coating (Fig. 10(b)), a similar trend with PEO coating was noticed at 2 N load but with more non-uniformity. For PEO-Clay coating, the width and depth of the wear tracks under 5 and 10 N loads were about 750 and 38 μm and 1100 and 55 μm, respectively. The maximum non-uniformity was observed in the case of PEO-Clay coating after wear testing at 10 N load. This behavior can be due to the higher roughness and occurrence of the abrasive and adhesive wear [56].

Figure 11 shows the SEM micrographs of the steel ball surfaces sliding against PEO and PEO-Clay coatings under different loads. The balls did not suffer from severe wear damage running against the PEO coating. They were almost smooth with some deep scoring on the worn surfaces. Under the 5 N load, the dominant mechanism of wear was abrasive. At 10 N load, extensive ploughing and detachment of debris suggested three-body abrasive wear for the clay-free coating. In addition, white wear debris on the sidelines of the ball surfaces and the existence of elements from the PEO coating (Mg, Al, P, Na) were obtained from EDS results of dashed line area of the worn ball surface (Fig. 12), thereby confirming the occurrence of an adhesive wear mode. It can be deduced that the activation of adhesive wear mechanism led to transfer of coating materials/debris from the coating to the balls. In Fig. 11 for PEO coating with clay particles, the abrasion with abrasive grooves was commonly observed under all loads. In order to get more information regarding the wear mechanisms at 10 N load, in which the contact surface of the ball became very rough, the worn surface of the steel ball and EDS results were also assessed, as presented in Fig. 13. In Region B, there was white wear debris, demonstrating the slight transfer of coating material to the ball according to the EDS results (Fig. 13(b)) and ball wear scar was uneven with many grooves. Nevertheless, abrasive wear between hard steel counter-face material (with hardness of around 900 HV) and PEO-Clay coating was fundamental mechanism in this region. In the Region C, dark contrast corresponds to material transfer by adhesive wear. The results of EDS analysis from this region is shown in Fig. 13(c), which revealed the presence of Mg, Al, Na, P and Si transferred from the PEO-Clay specimen along with Fe and Cr from the steel ball. The presence of oxygen is also detected due to the oxidation of surfaces [45]. In the case of Region D for worn steel ball and EDS results of this area in Fig. 13(d), only the elements Mg, O and Al can be observed and there is no Fe peak. So, the coating removal process is dominated by heavy and localized plastic deformation [57]. Indeed, due to less hardness of MgO than steel ball, the outer porous layers of the coatings during sliding were removed and stuck to the counterpart. In addition, by examination of this region, it may be concluded that magnesium oxide is formed on the worn surface of the ball during wear test. Furthermore, oxidative wear mechanism is obvious [48]. Also, Region D displayed a typical severe adhesive wear morphology, which was

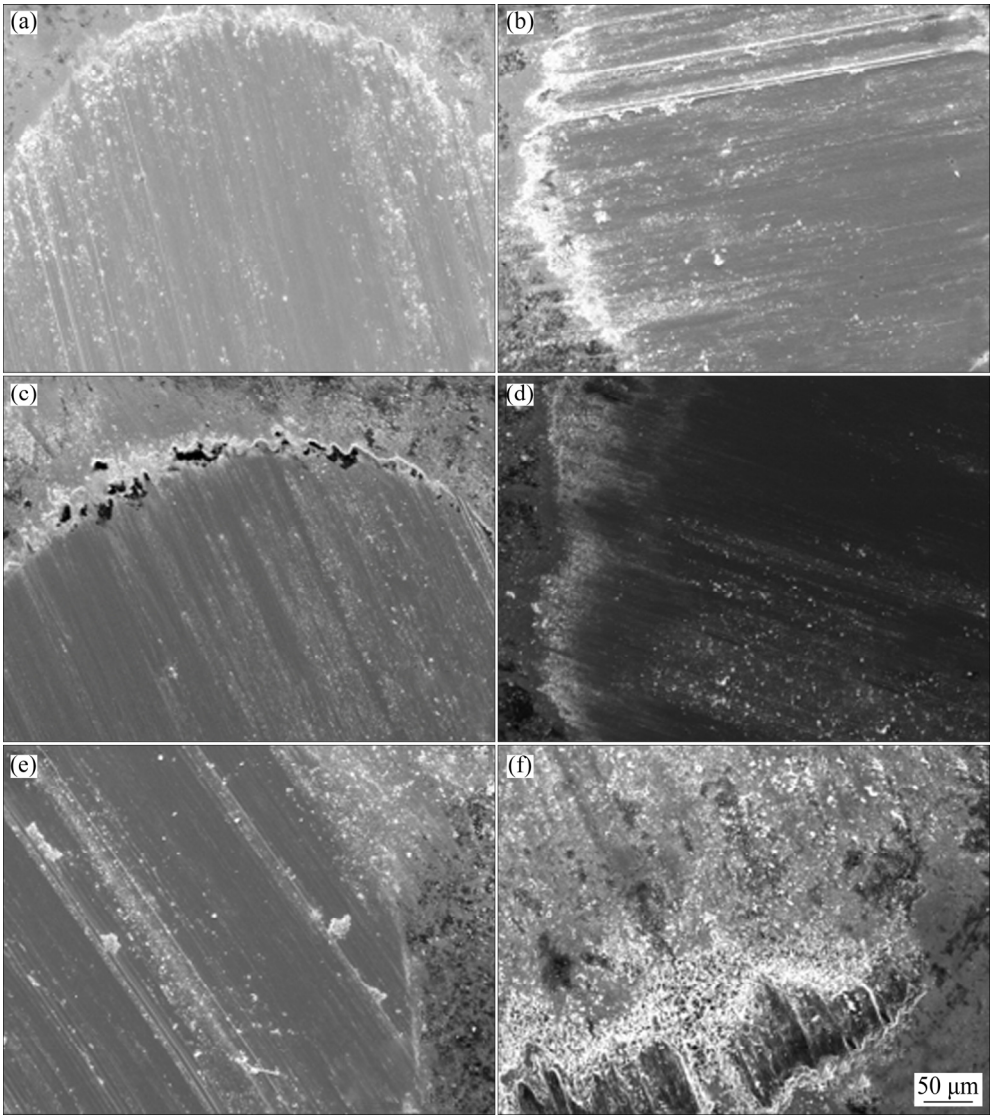

Fig. 11 SEM micrographs of steel ball wear tracks against PEO (a, c, e) and PEO-Clay (b, d, f) coatings under loads of 2 N (a, b), 5 N (c, d) and 10 N (e, f)

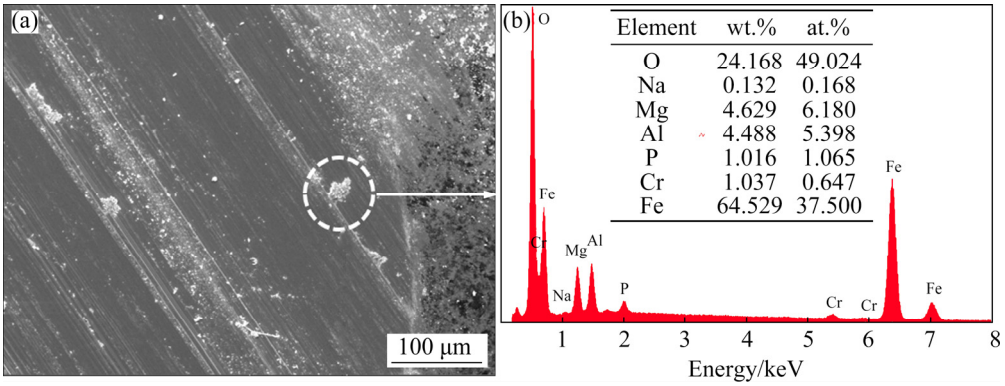

Element	wt.%	at.%
O	24.168	49.024
Na	0.132	0.168
Mg	4.629	6.180
Al	4.488	5.398
P	1.016	1.065
Cr	1.037	0.647
Fe	64.529	37.500

Fig. 12 SEM image (a) and EDS spectrum (b) of steel ball wear track against PEO coating under load of 10 N

ascribed in the study of ZHANG et al [49] to the typical influence of "instantaneous welding" because of the high temperatures in the contact area between the steel ball and specimen. This indicates that the PEO-Clay coating in this area is completely damaged.

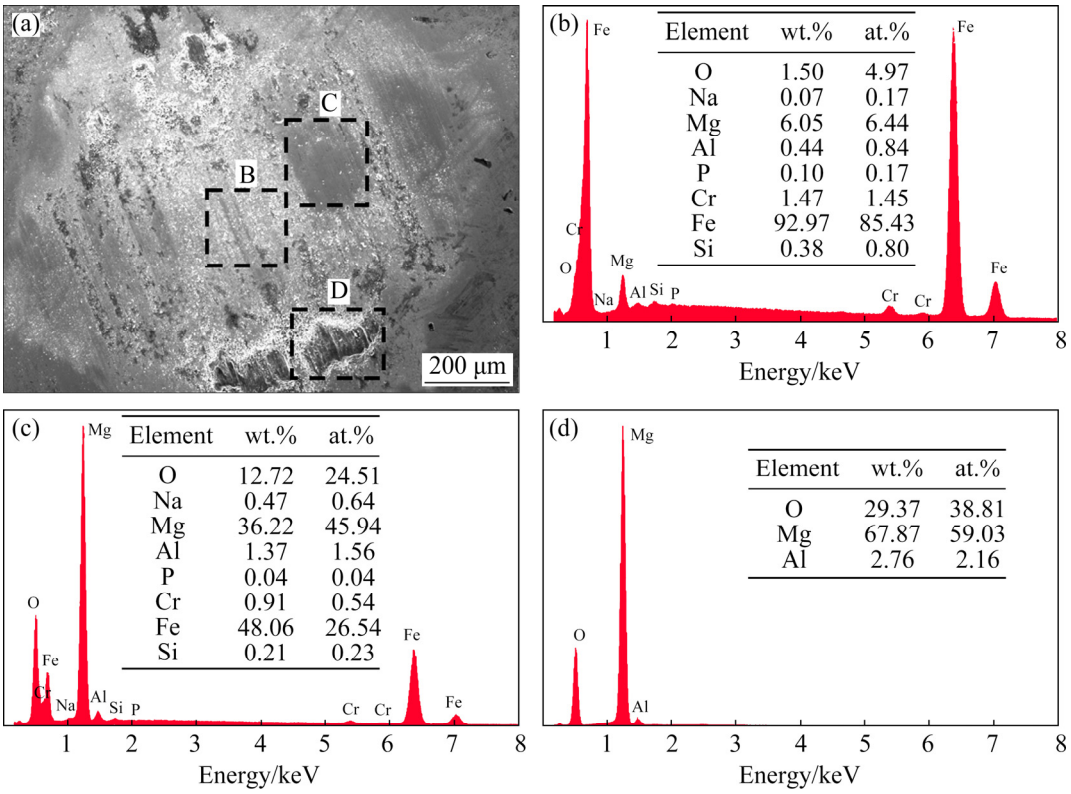

Fig. 13 SEM image of steel ball wear track against PEO-Clay coating under load of 10 N (a) and EDS spectra of Areas B (b), C (c) and D (d)

3.4 Corrosion performance

In this work, the corrosion performance of PEO and PEO-Clay coatings was evaluated by open circuit potential (OCP) behavior (Fig. 14), potentiodynamic polarization (Fig. 15) and electrochemical impedance spectroscopy (EIS) measurement (Fig. 16).

For AM50 alloy, the φ_{ocp} values initially increased and then decreased slowly and followed by a steady state condition. The increase and decrease of the potential can be related to the formation and dissolution of the $Mg(OH)_2$ film in the presence of Cl^- ions [58].

The results reveal that the PEO coating with and without clay particles did improve the OCP values when compared to the AM50 substrate. Fluctuations in the OCP data of coated specimens were observed during the early stages of immersion. Rapid decrease of the OCP values of coatings may be due to the penetration of the solution into the pores [59]. Among different tested specimens, the PEO-Clay exhibited the highest OCP, which means the lower corrosion tendency of this coating.

The corrosion potential (φ_{corr}) and corrosion current density (J_{corr}) values were extracted from the

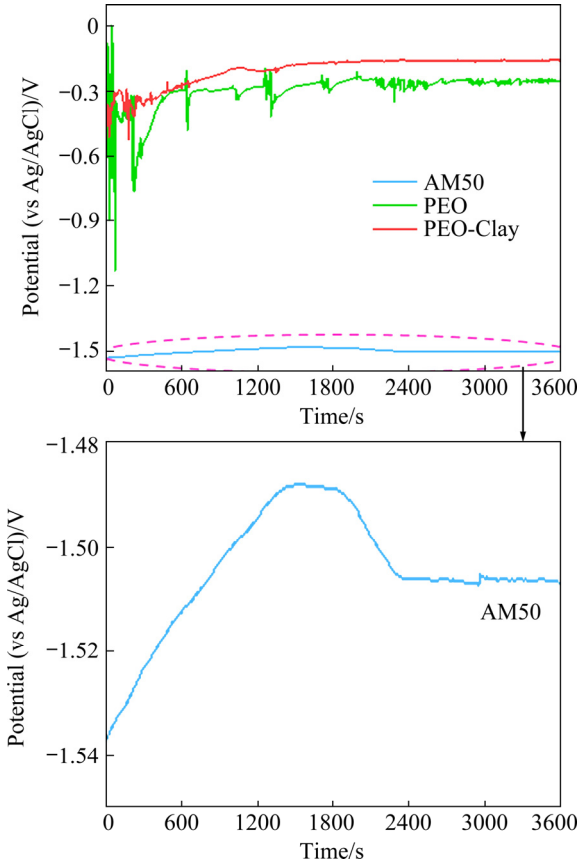

Fig. 14 OCP variation of substrate and coated samples in 0.5 wt.% NaCl solution

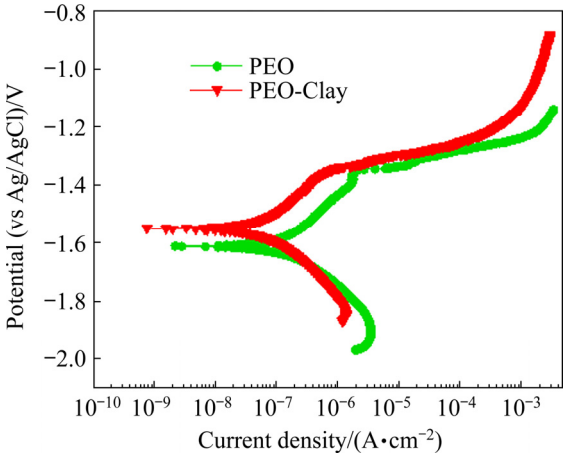

Fig. 15 Polarization curves of coated samples in 0.5 wt.% NaCl solution

polarization plots and listed in Table 3. The hydrogen reduction and the dissolution of magnesium are the main cathodic and anodic reactions, respectively [30]. As can be seen, from polarization curves, the corrosion current density of the coating loaded with clay particles was lower than that obtained for PEO coating. These results are in accordance with previous findings [29,30] in the case of clay-incorporated coating in phosphate PEO treatments. Other than oxidation coatings, positive effect of clay particles in improvement of corrosion resistance of polymeric composites [60], sol gel coatings [61] and bioactive nano-composites [62] has been also confirmed. It needs to note that the corrosion current density obtained for both coatings was lower than that of the cold forging/PEO [63] and higher than that of cold spray/PEO [64] duplex treated coatings.

In order to obtain more details on the corrosion process, the EIS evaluations were carried out on the coated specimens. Figure 16 shows the Nyquist and Bode curves of different coatings. Similar shapes of the Nyquist and Bode plots confirmed that similar results and corresponding mechanism of corrosion

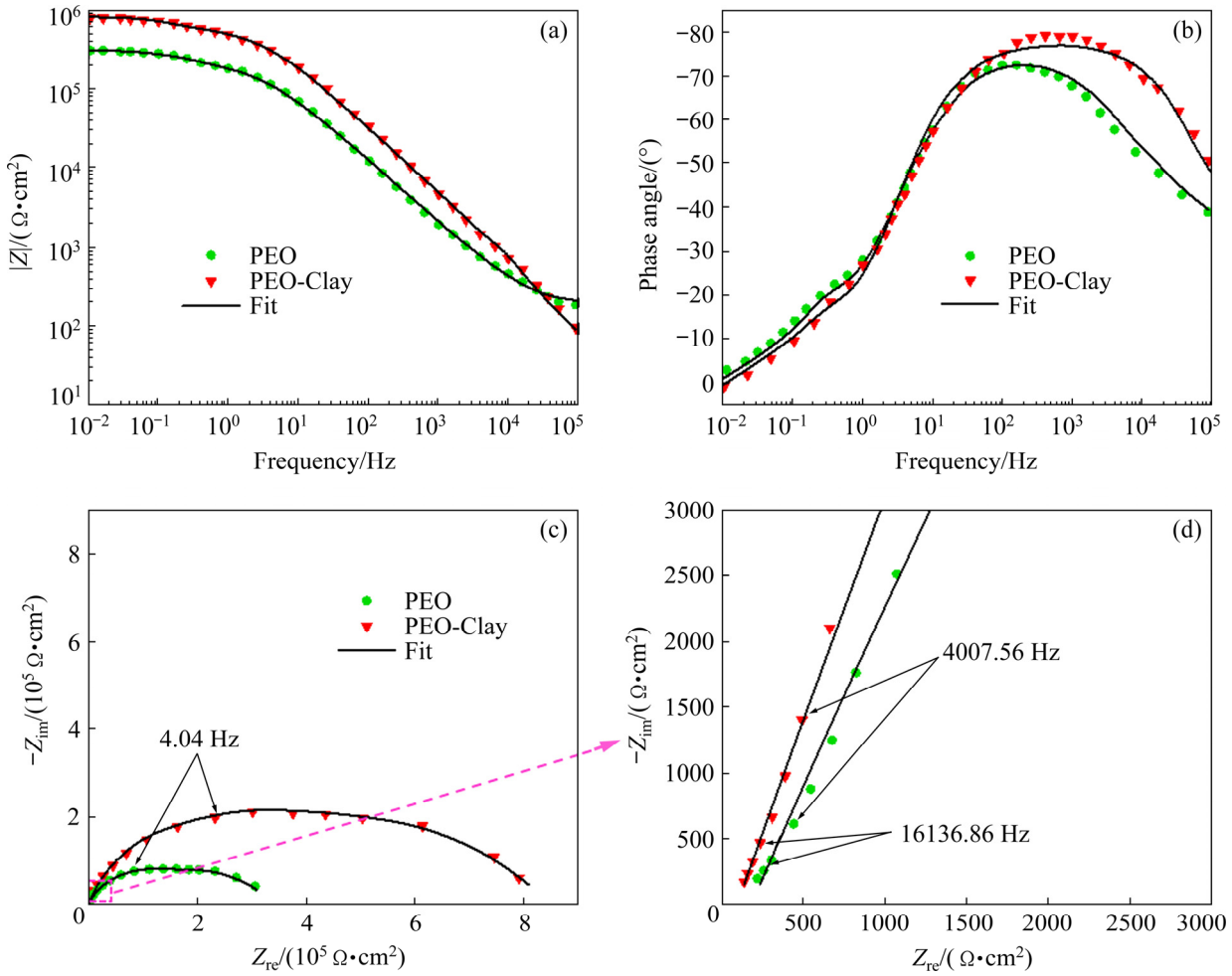

Fig. 16 Bode (a), phase angle (b) and Nyquist (c, d) diagrams of two coated samples after 1 h immersion in 0.5 wt.% NaCl solution

Table 3 Corrosion current densities and corrosion potentials obtained for PEO and PEO-Clay coatings from polarization tests using Tafel extrapolation method

Sample	J_{corr}/(nA·cm^{-2})	φ_{corr} (vs Ag/AgCl)/V
PEO	99.6	−1.6176
PEO-Clay	32.8	−1.5459

process can be presented for the coatings with and without clay particles. The high frequency and low frequency spectra correspond to the outer porous layer and the inner compact layer of the plasma electrolyte oxidation coatings, respectively [65]. Dense inner layer plays the most important role in corrosion resistance of the coating [66]. Based on the Nyquist curves, the appearance of a larger capacitive loop for the PEO-Clay coating demonstrated that the addition of clay particles improved the corrosion resistance of the PEO coatings. Also, the more increase of the phase angle aperture after applying the PEO-Clay coating on the Mg substrate can be attributed to the more protective performance of this coating than coating without particle [3]. This behavior can be due to the formation of more closed pores and compact inner layer of the PEO coating with clay particles. Generally, it has been reported that the corrosion resistance of PEO coatings is related to the porosity [67]. Lower porosity and smaller pore size can lead to an enhancement in the corrosion resistance. Thus, superior corrosion resistance of the PEO-Clay coating can be due to the formation of smaller pores (Fig. 2(b)) which decreased the penetration of the solution to the interface. On the other hand, the formation of big pores and higher porosity of PEO coating can lead to the penetration of solution into the pores and acceleration of the corrosion [67].

Also, the formation of the amorphous phase in the PEO-Clay coating can be another positive factor in improving the corrosion resistance [68]. It is known that the amorphous materials exhibit a very good corrosion resistance due to lack of long-range order characteristics [69]. It has been reported that the amorphous layers helped to improve the corrosion resistance of the PEO coatings on Al [70] and Mg [59] alloys. It has also been found that the amorphous layers act as diffusion barriers and improve the corrosion resistance [70].

For better understanding of the overall corrosion properties of the coatings, the impedance spectra were fitted by an appropriate electrical circuit, as shown in Fig. 17. The choice of the circuit was a compromise between a reasonable fitting of the experimental values and an appropriate description of the electrochemical system by maintaining the number of circuit elements at a minimum [71]. Based on the Nyquist plots (Fig. 16(c)), the large capacitive loops at low frequencies correspond to the more compact inner layers. In contrast, the small capacitive loops at high frequencies are related to the outer porous layers. The results of the fitting are reported in Table 4. Different parameters are used to describe different components of the coatings. In this circuit, R_s represents solution resistance; R_{in} and R_{out} correspond to the inner barrier layer resistance and outer layer resistance, respectively. CPE_{in} and CPE_{out} are related to the constant phase elements of the inner layer and the outer layer, respectively [72]. The previous studies [29,30] on long-term EIS measurements for PEO and PEO-Clay coated samples in phosphate electrolyte have shown that in the beginning of immersion, two well-defined time constants in low frequency and high frequency are observed which were relevant to the inner and outer layers, respectively. In agreement with these findings, it can be said that in this study after 1 h immersion, two time constants were recognized for both coatings: the time constant in low frequency which was related to the inner layer and the time constant in high frequency which was assigned to the outer layer. Figure 17 shows the equivalent circuit used in this work. In Table 4, the higher CPE value of the PEO coating without clay particles can be related to the higher porosity [73], so the low charge transfer behavior of the PEO-Clay coating is

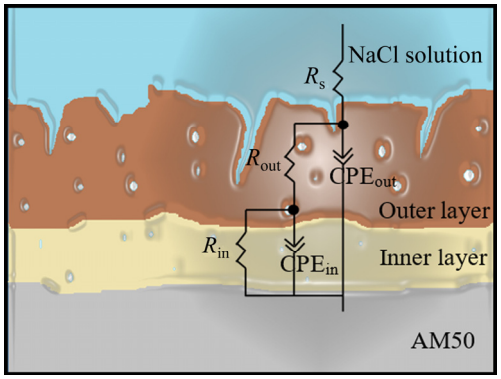

Fig. 17 Schematic representation of equivalent circuit of coatings degradation

Table 4 Fitting results of experimental data for coated samples after EIS tests

Sample	R_s/ ($\Omega\cdot cm^2$)	R_{out}/ ($\Omega\cdot cm^2$)	R_{in}/ ($\Omega\cdot cm^2$)	CPE_{out}/ ($\mu F\cdot cm^{-2}\cdot S^{n-1}$)	CPE_{in}/ ($\mu F\cdot cm^{-2}\cdot S^{n-1}$)	n_{out}	n_{in}
PEO	183.6	0.88×10^5	2.24×10^5	0.5	7.97	0.79	0.98
PEO-Clay	90.67	1.92×10^5	5.9×10^5	0.15	4.19	0.82	0.95

due to its lower porosity. The impedance modulus at low frequency for PEO and PEO-Clay coatings was 312.96 and 782.65 $k\Omega\cdot cm^2$, respectively, which was more than that of PEO coating with other additives like phosphate [74] and less than that reported for the flash-PEO [75] or polymeric coatings [76].

4 Conclusions

(1) Clay particles with low melting point were successfully incorporated into the PEO coatings. The addition of clay particles led to the formation of bigger closed pores on the surface and higher roughness.

(2) The wear examinations showed that the PEO coating with and without clay particles exhibited very similar wear rate and friction coefficient at 2 N load. However, under 5 and 10 N loads, the coating with clay particles showed higher wear rate and higher friction coefficient.

(3) SEM morphology of the worn surfaces revealed that activation of a three-body abrasive wear mechanism led to high wear rates for the coating with clay particles. The occurrence of the adhesive wear was also confirmed based on the EDS results for the coatings tested at 5 and 10 N. The SEM evaluations of the worn surfaces of the balls showed that the level of wear was increased by increasing the loads.

(4) The addition of clay particles improved the corrosion resistance by enhancing the barrier resistance of the aluminate-based PEO coatings. However, the effect of clay was not so remarkable on the corrosion of these coatings. Also, the corrosion improvement of the PEO-Clay composite coating was attributed to the formation of amorphous phase in the surface.

(5) The addition of clay micro particles can deteriorate the wear resistance of Mg alloys because of the increased roughness and brittleness of the PEO coatings. However, reactive incorporation of the clay particles into the aluminate-based PEO coatings improved the corrosion resistance of AM50.

Acknowledgments

The authors would like to give their sincere thanks to Mr. Ulrich BURMESTER, Mr. Volker HEITMANN and Mr. Gert WIESE for their technical supports. One of authors (Masoud ATAPOUR) would like to acknowledge the financial support from Invited Collaborative Research Program (ICRP), Center for International Scientific Studies and Collaboration, Ministry of Science, Research and Technology of Iran.

References

[1] NASIRIVATAN Hadi, EBRAHIMI-KAHRIZSANGI Reza, KASIRI ASGARANI Masoud. Tribological performance of PEO-WC nanocomposite coating on Mg alloys deposited by plasma electrolytic oxidation [J]. Tribology International, 2016, 98: 253−260.

[2] REHMAN Zeeshan Ur, UZAIR Muhammad, LIM Hyung Tae, KOO Bon Heun. Structural and electrochemical properties of the catalytic CeO_2 nanoparticles-based PEO ceramic coatings on AZ91 Mg alloy [J]. Journal of Alloys and Compounds, 2017, 726: 284−294.

[3] DAROONPARVAR Mohammadreza, YAJID Muhamad Azizi Mat, YUSOF Noordin Mohd, BAKHSHESHI-RAD Hamid Reza. Preparation and corrosion resistance of a nanocomposite plasma electrolytic oxidation coating on Mg−1%Ca alloy formed in aluminate electrolyte containing titania nano-additives [J]. Journal of Alloys and Compounds, 2016, 688: 841−857.

[4] ROSE A Razal, MANISEKAR K, BALASUBRAMANIAN V. Effect of axial force on microstructure and tensile properties of friction stir welded AZ61A magnesium alloy [J]. Transactions of Nonferrous Metals Society of China, 2011, 21: 974−984.

[5] JOTHI V, ADESINA Akeem Yusuf, RAHMAN Mohammad Mizanur, KUMAR A Madhan, RAM J S. Improved adhesion and corrosion resistant performance of polyurethane coatings on anodized Mg alloy for aerospace applications [J]. JMEP, 2020, 29: 2586−2596.

[6] LI Xiao-jie, YIN Shao-hui, HUANG Shuai, LUO H U, TANG Qing-chun. Fabrication of durable superhydrophobic Mg alloy surface with water-repellent, temperature-resistant, and self-cleaning properties [J]. Vacuum, 2020, 173: 109172.

[7] REHMAN Zeeshan Ur, JEONG Chanyoung, CHOI Dong Jin.

Effect of NaOH concentration on the microstructure and mechanical properties of the PEO coatings on Mg−Al3−Zn1 alloy [J]. Materials Science Forum, 2020, 977: 83−89.

[8] LU Xiao-peng, BLAWERT Carsten, TOLNAI Domonkos, SUBROTO Tungky, KAINER Karl Ulrich, ZHANG Tao, WANG Fu-hui, ZHELUDKEVICH Mikhail L. 3D reconstruction of plasma electrolytic oxidation coatings on Mg alloy via synchrotron radiation tomography [J]. Corrosion Science, 2018, 139: 395−402.

[9] BULING Anna, ZERRER Joerg. Increasing the application fields of magnesium by ultraceramic: Corrosion and wear protection by plasma electrolytical oxidation (PEO) of Mg alloys [J]. Surface and Coating Technology, 2019, 369: 142−155.

[10] YAMAUCHI Naohiko, DEMIZU Kei, UEDA Nobuhiro, CUONG Nguyen K, SONE Takumi, HIROSE Yukio. Friction and wear of DLC films on magnesium alloy [J]. Surface and Coating Technology, 2005, 193: 277−282.

[11] DAROONPARVAR Mohammadreza, YAJID Muhamad Azizi Mat, GUPTA Rajeev Kumar, YUSOF Noordin Mohd, BAKHSHESHI-RAD Hamid Reza, GHANDVAR Hamid Reza, GHASEMI Ehsan. Antibacterial activities and corrosion behavior of novel PEO/nanostructured ZrO_2 coating on Mg alloy [J]. Transactions of Nonferrous Metals Society of China, 2018, 28: 1571−1581.

[12] WU Wei-wei, WANG Zi-yuan, ZANG Si-tian, YU Xiao-ming, YANG Hua-zhe, CHANG Shi-jie. Research progress on surface treatments of biodegradable Mg alloys: A review [J]. ACS Omega, 2020, 5: 941−947.

[13] YIN Zheng-zheng, QI Wei-chen, ZENG Rong-chang, CHEN Xiao-bo, GU Chang-dong, GUAN Shao-kang, ZHENG Yu-feng. Advances in coatings on biodegradable magnesium alloys [J]. Journal of Magnesium and Alloys, 2020, 8: 42−65.

[14] ATAPOUR Masoud, BLAWERT Carsten, ZHELUDKEVICH Mikhail L. The wear characteristics of CeO_2 containing nanocomposite coating made by aluminate-based PEO on AM 50 magnesium alloy [J]. Surface and Coatings Technology, 2019, 357: 626−637.

[15] HUSSEIN Mohamed Abdrabou, ANKAH Nestor, KUMAR A Madhan, ABDOL AZEEM Mohammed, SARAVANAN S, SOROUR Ahmad A, AL AQEELI Nasser. Mechanical, biocorrosion, and antibacterial properties of nanocrystalline TiN coating for orthopedic applications [J]. Ceramics International, 2020, 46: 18573−18583.

[16] AN Ling-yun, MA Ying, YAN Xiao-xu, WANG Sheng, WANG Zhan-ying. Effects of electrical parameters and their interactions on plasma electrolytic oxidation coatings on aluminum substrates [J]. Transactions of Nonferrous Metals Society of China, 2020, 30: 883−895.

[17] BARATI DARBAND Ghasem, ALIOFKHAZRAEI Mahmood, HAMGHALAM Parsa, VALIZADE Nima. Plasma electrolytic oxidation of magnesium and its alloys: Mechanism, properties and applications [J]. Journal of Magnesium and Alloys, 2017, 5: 74−132.

[18] LI Chang-yang, FENG Xiao-lei, FAN Xiao-li, YU Xiao-tong, YIN Zheng-zheng, KANNAN M bobby, CHEN Xiao-bo, GUAN Shao-kang, ZHANG Jun, ZENG Rong-chang. Corrosion and wear resistance of micro-arc oxidation composite coatings on magnesium alloy AZ31 — The influence of inclusions of carbon spheres [J]. Advanced Engineering Materials, 2019, 21: 1900446.

[19] CUI Lan-yue, GAO Shang-dong, LI Ping-ping, ZENG Rong-chang, ZHANG Fen, LI Shuo-qi, HAN En-hou. Corrosion resistance of a self-healing micro-arc oxidation/ polymethyltrimethoxysilane composite coating on magnesium alloy AZ31 [J]. Corrosion Science, 2017, 118: 84−95.

[20] ZHANG Zhao-qi, WANG Li, ZENG Mei-qi, ZENG Rong-chang, KANNAN M Bobby, LIN Cun-guo, ZHENG Yu-feng. Biodegradation behavior of micro-arc oxidation coating on magnesium alloy-from a protein perspective [J]. Bioactive Materials, 2020, 5: 398−409.

[21] LI Chang-yang, FAN Xiao-li, CUI Lan-yue, ZENG Rong-chang. Corrosion resistance and electrical conductivity of a nano ATO-doped MAO/methyltrimethoxysilane composite coating on magnesium alloy AZ31 [J]. Corrosion Science, 2020, 168: 108570.

[22] LI Chang-yang, YU Chi, ZENG Rong-chang, ZHANG Bo-cheng, CUI Lan-yue, WAN Jun, XIA Yang. In vitro corrosion resistance of a Ta_2O_5 nanofilm on MAO coated magnesium alloy AZ31 by atomic layer deposition [J]. Bioactive Materials, 2020, 5: 34−43.

[23] DAROONPARVAR Mohammadreza, KHAN Mohammad Umar Farooq, SAADEH Y, KAY Charls M, GUPTA Rajeev, KASAR Ashish Kumar, KUMAR Pankaj, MISRA M, MENEZES Pradeep L, BAKHSHESHI-RAD Hamidreza. Enhanced corrosion resistance and surface bioactivity of AZ31B Mg alloy by high pressure cold sprayed monolayer Ti and bilayer Ta/Ti coatings in simulated body fluid [J]. Materials Chemistry and Physics, 2020, 256: 123627.

[24] RAO Yu-qin, WANG Qun, OKA Daisuke, RAMACHANDRAN Chidambaram Seshadri. On the PEO treatment of cold sprayed 7075 aluminum alloy and its effects on mechanical, corrosion and dry sliding wear performances thereof [J]. Surface and Coatings Technology, 2020, 383: 125271.

[25] MARTIN Julien, AKODA Komlan Elom, NTOMPROUGKIDIS Vitalis, FERRY Olivier, MAIZERAY A, BASTIEN A, BRENOT P, EZO'O G, HENRION Gerard. Duplex surface treatment of metallic alloys combining cold-spray and plasma electrolytic oxidation technologies [J]. Surface and Coatings Technology, 2020, 392: 125756.

[26] SHENG Lu, WANG Ze-xin, JING Chen, ZHOU Xiao-song. Optimization of dual electrolyte and characteristic of micro-arc oxidation coating fabricated on ZK60 Mg alloy [J]. Transactions of Nonferrous Metals Society of China, 2011, 21: 929−935.

[27] DEHNAVI Vahid, BINNS W Jeffray, NOEL J J, SHOESMITH David W, LUAN B L. Growth behaviour of low-energy plasma electrolytic oxidation coatings on a magnesium alloy [J]. Journal of Magnesium and Alloys, 2018, 6: 229−237.

[28] YING Qin, WU Guo-hua, ATRENS Andrej, ZHANG Xiao-long, ZHANG Liang, DING Wen-jiang. Effect of NaOH concentration on microstructure and corrosion resistance of MAO coating on cast Al−Li alloy [J]. Transactions of Nonferrous Metals Society of China, 2021, 31: 913−924.

[29] LU Xiao-peng, BLAWERT Carsten, KAINER Karl Ulrich, ZHANG Tao, WANG Fu-hui, ZHELUDKEVICH Mikhail. Influence of particle additions on corrosion and wear resistance of plasma electrolytic oxidation coatings on Mg alloy [J]. Surface and Coatings Technology, 2018, 352: 1−14.

[30] LU Xiao-peng, SAH Santosh Prasad, SCHARNAGL Nico, STöRMER Michael, STARYKEVICH Maksim, MOHEDANO Marta, BLAWERT Carsten, ZHELUDKEVICH Mikhail L, KAINER Karl Ulrich. Degradation behavior of PEO coating on AM50 magnesium alloy produced from electrolytes with clay particle addition [J]. Surface and Coatings Technology, 2015, 269: 155−169.

[31] LOU Bih-show, LEE Jyh-wei, TSENG Chuan-ming, LIN Yi-yuan, YEN Chien-an. Mechanical property and corrosion resistance evaluation of AZ31 magnesium alloys by plasma electrolytic oxidation treatment: Effect of MoS_2 particle addition [J]. Surface and Coatings Technology, 2018, 350: 813−822.

[32] RAPHEAL G, KUMAR Subodh, SCHARNAGL Nico, BLAWERT Carsten. Effect of current density on the microstructure and corrosion properties of plasma electrolytic oxidation (PEO) coatings on AM50 Mg alloy produced in an electrolyte containing clay additives [J]. Surface and Coatings Technology, 2016, 289: 150−164.

[33] FATTAH-ALHOSSEINI Arash, CHAHARMAHALI Razieh, BABAEI Kazem. Effect of particles addition to solution of plasma electrolytic oxidation (PEO) on the properties of PEO coatings formed on magnesium and its alloys: A review [J]. Journal of Magnesium and Alloys, 2020, 8: 799−818.

[34] BLAWERT Carsten, SAH Santosh Prasad, LIANG Jun, HUANG Yuanding, HöCHE Daniel. Role of sintering and clay particle additions on coating formation during PEO processing of AM50 magnesium alloy [J]. Surface and Coatings Technology, 2012, 213: 48−58.

[35] GUO Jie, WANG Li-ping, LIANG Jun, XUE Qun-ji, YAN Feng-yuan. Tribological behavior of plasma electrolytic oxidation coating on magnesium alloy with oil lubrication at elevated temperatures [J]. Journal of Alloys and Compounds, 2009, 481: 903−909.

[36] MASHTALYAR Dmitry Valerevich, SINEBRYUKHOV Sergey L, IMSHINETSKIY Igor M, GNEDENKOV Andrey S, NADARAIA Konstantine Vakhtangovich, USTINOV Alexander Yu, GNEDENKOV Sergey Vasilievich. Hard wearproof PEO-coatings formed on Mg alloy using TiN nanoparticles [J]. Applied Surface Science, 2020, 503: 144062.

[37] TANG Hui, HAN Yu, WU Tao, TAO Wei, JIAN Xian, WU Yun-feng, XU Fang-jun. Synthesis and properties of hydroxyapatite-containing coating on AZ31 magnesium alloy by micro-arc oxidation [J]. Applied Surface Science, 2017, 400: 391−404.

[38] LU Xiao-peng, MOHEDANO Marta, BLAWERT Carsten, MATYKINA Endzhe, ARRABAL Raul, KAINER Karl Ulrich, ZHELUDKEVICH Mikhail L. Plasma electrolytic oxidation coatings with particle additions—A review [J]. Surface and Coatings Technology, 2016, 307: 1165−1182.

[39] KHAN Raja, YEROKHIN Aleksey, PILKINGTON T, LEYLAND A, MATTHEWS A. Residual stresses in plasma electrolytic oxidation coatings on Al alloy produced by pulsed unipolar current [J]. Surface and Coatings Technology, 2005, 200: 1580−1586.

[40] TOULABIFARD Amirhossein, RAHMATI Maryam, RAEISSI Keyvan, HAKIMIZAD Amin, SANTAMARIA Monica. The effect of electrolytic solution composition on the structure, corrosion, and wear resistance of PEO coatings on AZ31 magnesium alloy [J]. Coatings, 2020, 10: 937.

[41] LIM Tae Seop, RYU Hyun Sam, HONG Seong-hyeon. Electrochemical corrosion properties of CeO_2-containing coatings on AZ31 magnesium alloys prepared by plasma electrolytic oxidation [J]. Corrosion Science, 2012, 62: 104−111.

[42] SAH Santosh Prasad, AOKI Yoshitaka, HABAZAKI Hiroki. Influence of phosphate concentration on plasma electrolytic oxidation of AZ80 magnesium alloy in alkaline aluminate solution [J]. Materials Transactions, 2010, 51: 94−102.

[43] LI Xi-jin, LIU Xing-yang, LUAN Ben-li. Corrosion and wear properties of PEO coatings formed on AM60B alloy in $NaAlO_2$ electrolytes [J]. Applied Surface Science, 2011, 257: 9135−9141.

[44] KHALILI S Mohammadreza Reza, TAVAKOLIAN M, SARABI A. Mechanical properties of nanoclay reinforced epoxy adhesive bonded joints made with composite materials [J]. Journal of Adhesion Science and Technology, 2010, 24: 1917−1928.

[45] RAPHEAL G, KUMAR Subodgh, BLAWERT Carsten, DAHOTRE Narendra B. Wear behavior of plasma electrolytic oxidation (PEO) and hybrid coatings of PEO and laser on MRI 230D magnesium alloy [J]. Wear, 2011, 271: 1987−1997.

[46] SHARIFI Hossein, ALIOFKHAZRAEI Mahmood, BRATAI DARBAND Ghasem, ROUHAGHDAM A Sabour. Tribological properties of PEO nanocomposite coatings on titanium formed in electrolyte containing ketoconazole [J]. Tribology International, 2016, 102: 463−471

[47] LI Ze-chao, WANG Yong-xin, CHENG Xiao-ying, ZENG Zhi-xiang, LI Jin-long, LU Xia, WANG Li-ping, XUE Qun-ji. Continuously growing ultrathick CrN coating to achieve high load-bearing capacity and good tribological property [J]. ACS Applied Materials & Interfaces, 2018, 10: 2965−2975.

[48] AYDIN Fatih, AYDAY Aysun, TURAN M Emre, ZENGIN Huseyin. Role of graphene additive on wear and electrochemical corrosion behaviour of plasma electrolytic oxidation (PEO) coatings on Mg–MWCNT nanocomposite [J]. Surface Engineering, 2020, 36: 791−799.

[49] ZHANG Yu-lin, CHEN Fei, ZHANG You, DU Cui-wei. Influence of graphene oxide additive on the tribological and electrochemical corrosion properties of a PEO coating prepared on AZ31 magnesium alloy [J]. Tribology International, 2020: 106135.

[50] SRINIVASAN P Bala, LIANG Jun, BLAWERT Carsten, DIETZEL W. Dry sliding wear behaviour of magnesium oxide and zirconium oxide plasma electrolytic oxidation coated magnesium alloy [J]. Applied Surface Science, 2010, 256: 3265−3273.

[51] MU Bo, WANG Qi-hua, WANG Ting-mei, WANG Hong-gang, JIAN Ling-qi. The friction and wear properties of clay filled PA66 [J]. Polymer Engineering & Science,

2008, 48: 203−209.

[52] DASARI Aravind, YU Zhong-zhen, MAI Yiu-wing, HU Guo-hua, VARLET Joel. Clay exfoliation and organic modification on wear of nylon 6 nanocomposites processed by different routes [J]. Composites Science and Technology, 2005, 65: 2314−2328.

[53] MINGO Baetriz, ARRABAL Raul, MOHEDANO Marta, PARDO A, MATYKINA E. Corrosion and wear of PEO coated AZ91/SiC composites [J]. Surface and Coatings Technology, 2017, 309: 1023−1032.

[54] ALIOFKHAZRAEI Mahmood, SHOJA GHARABAGH Ramin, TEIMOURI M, AHMADZADEH Mohammad, BARATI DARBAND Ghasem, HASANNEJAD Hossein. Ceria embedded nanocomposite coating fabricated by plasma electrolytic oxidation on titanium [J]. Journal of Alloys and Compounds, 2016, 685: 376−383.

[55] SRINATH Gajapathy, GNANAMOORTHY R. Effect of organoclay addition on the two-body abrasive wear characteristics of polyamide 6 nanocomposites [J]. Journal of Materials Science, 2007, 42: 8326−8333.

[56] WHITE Leon, KOO Youngmi, NERALLA Sudheer, SANKAR Jagannathan, YUN Yeoheung. Enhanced mechanical properties and increased corrosion resistance of a biodegradable magnesium alloy by plasma electrolytic oxidation (PEO) [J]. Materials Science and Engineering B, 2016, 208: 39−46.

[57] TONELLI Lavinia, PEZZATO Luca, DOLCET Paolo, DABALA Manuele, MARTINI Carla. Effects of graphite nano-particle additions on dry sliding behaviour of plasma-electrolytic-oxidation-treated EV31A magnesium alloy against steel in air [J]. Wear, 2018, 404: 122−132.

[58] WANG Lei, SHINOHARA Tadashi, ZHANG Bo-ping. Corrosion behavior of Mg, AZ31, and AZ91 alloys in dilute NaCl solutions [J]. Journal of Solid State Electrochemistry, 2010, 14: 1897−1907.

[59] ARRABAL Raul, MATYKINA Endzhe, VIEJO Fernando, SKELDON P, THOMPSON George E. Corrosion resistance of WE43 and AZ91D magnesium alloys with phosphate PEO coatings [J]. Corrosion Science, 2008, 50: 1744−1752.

[60] RAJU Annu, LAKSHMI Viji, PRATAAP R K Vishnu, RESMI V G, RAJAN T P D, PAVITHRAN C, PRASAD Vadakkethonippurathu Sivankuttynair, MOHAN Subramanian. Adduct modified nano-clay mineral dispersed polystyrene nanocomposites as advanced corrosion resistance coatings for aluminum alloys [J]. Applied Clay Science, 2016, 126: 81−88.

[61] CALLONE Emanuela, CECCATO Riccardo, DEFLORIAN Flavio, FEDEL Michele, DIRE Sandra. Filler−matrix interaction in sodium montmorillonite−organosilica nanocomposite coatings for corrosion protection [J]. Applied Clay Science, 2017, 150: 81−88.

[62] USMANIYA U Mehana, THAMPI V V Anusha, SUBRAMANIAN B. Electrophoretic deposition of bioactive glass-nanoclay nanocomposites on titanium [J]. Applied Clay Science, 2019, 167: 1−8.

[63] CHEN Ling-ling, GU Yan-hong, LIU Lu, LIU Shu-jing, HOU Bin-bin, LIU Qi, DING Hai-yang. Effect of ultrasonic cold forging technology as the pretreatment on the corrosion resistance of MAO Ca/P coating on AZ31B Mg alloy [J]. Journal of Alloys and Compounds, 2015, 635: 278−288.

[64] DAROONPARVAR Mohammadreza, KHAN Mohammad Umar Farooq, SAADEH Y, KAY Charles M, KASAR Ashish Kumar, KUMAR Pankaj, ESTEVES Luiza, MISRA M, MENEZES Pradeep L, KALVALA P R. Modification of surface hardness, wear resistance and corrosion resistance of cold spray Al coated AZ31B Mg alloy using cold spray double layered Ta/Ti coating in 3.5 wt.% NaCl solution [J]. Corrosion Science, 2020, 176: 109029.

[65] ZHAI Da-jun, FENG Ke-qin. Preparation of micro/nano-structured ceramic coatings on Ti6Al4V alloy by plasma electrolytic oxidation process [J]. Transactions of Nonferrous Metals Society of China, 2019, 29: 2546−2555.

[66] DAAVARI Morteza, ATAPOUR Masoud, MOHEDANO Marta, ARRABAL Raul, MATYKINA Endzhe, TAHERIZADEH Aboozar. Biotribology and biocorrosion of MWCNTs-reinforced PEO coating on AZ31B Mg alloy [J]. Surfaces and Interfaces, 2020: 100850.

[67] CUI Lan-yue, ZENG Rong-chang, GUAN Shao-kang, QI Wei-chen, ZHANG Fen, LI Shuo-qi, HAN En-hou. Degradation mechanism of micro-arc oxidation coatings on biodegradable Mg−Ca alloys: The influence of porosity [J]. Journal of Alloys and Compounds, 2017, 695: 2464−2476.

[68] MORI Yoichi, KOSHI Akihiko, LIAO Jin-sun, ASOH Hidetaka, ONO Sachiko. Characteristics and corrosion resistance of plasma electrolytic oxidation coatings on AZ31B Mg alloy formed in phosphate–silicate mixture electrolytes [J]. Corrosion Science, 2014, 88: 254−262.

[69] ZHU Zhun-da, TU Wen-bin, CHENG Yu-lin, CHENG Ying-liang. The formation of metallic W and amorphous phase in the plasma electrolytic oxidation coatings on an Al alloy from tungstate-containing electrolyte [J]. Surface and Coatings Technology, 2019, 361: 176−187.

[70] NIE Xie, MELETIS Efstathios I, JIANG J C, LEYLAND A, YEROKHIN Aleksey L, MATTHEWS A. Abrasive wear/corrosion properties and TEM analysis of Al_2O_3 coatings fabricated using plasma electrolysis [J]. Surface and Coatings Technology, 2002, 149: 245−251.

[71] HUSSEIN Riyad, NORTHWOOD Derek, NIE Xie. The effect of processing parameters and substrate composition on the corrosion resistance of plasma electrolytic oxidation (PEO) coated magnesium alloys [J]. Surface and Coatings Technology, 2013, 237: 357−368.

[72] WANG Zhi-hu, ZHANG Ju-mei, YAN Li, BAI Li-jing, ZHANG Guo-jun. Enhanced corrosion resistance of micro-arc oxidation coated magnesium alloy by superhydrophobic Mg−Al layered double hydroxide coating [J]. Transactions of Nonferrous Metals Society of China, 2019, 29: 2066−2077.

[73] AKBARI Ehsan, DI FRANCO Francesco, CERAOLO Paolo, RAEISSI Keyvan, SANTAMARIA Monica, HAKIMIZAD Amin. Electrochemically-induced TiO_2 incorporation for enhancing corrosion and tribocorrosion resistance of PEO coating on 7075 Al alloy [J]. Corrosion Science, 2018, 143: 314−328.

[74] LI Zhi-jun, REN Qing-hui, WANG Xue-xia, KUANG Qing, JI De-bin, YUAN Rui-xia, JING Xiao-yan. Effect of phosphate additive on the morphology and anti-corrosion performance of plasma electrolytic oxidation coatings on

magnesium−lithium alloy [J]. Corrosion Science, 2019, 157: 295−304.

[75] WIERZBICKA Ewa, VAGHEFINAZARI Bahram, LAMAKA Sviatlana V, ZHELUDKEVICH Mikhail L, MOHEDANO Marta, MORENO L, VISSER Peter, RODRIGUEZ A, VELASCO J, ARRABAL Raul, MATYKINA Endzhe. Flash-PEO as an alternative to chromate conversion coatings for corrosion protection of Mg alloy [J]. Corrosion Science, 2021, 180: 109189.

[76] LIU Min, MAO Xu-hui, ZHU Hua, LIN An, WANG Di-hua. Water and corrosion resistance of epoxy–acrylic–amine waterborne coatings: Effects of resin molecular weight, polar group and hydrophobic segment [J]. Corrosion Science, 2013, 75: 106−113.

等离子体电解氧化 AM 50 镁合金表面含黏土涂层的磨损与腐蚀行为

Farideh DAVOODI[1], Masoud ATAPOUR[1,2], Carsten BLAWERT[2], Mikhail ZHELUDKEVICH[2,3]

1. Department of Materials Engineering, Isfahan University of Technology, Isfahan 84156-83111, Iran;
2. MagIC−Magnesium Innovation Centre, Institute of Materials Research, Helmholtz Zentrum Geesthacht, Max-Plank-Str. 1, 21502 Geesthacht, Germany;
3. Faculty of Engineering, University of Kiel, Kaiserstrasse 2, 24143 Kiel, Germany

摘　要：采用等离子体电解氧化(PEO) 在 AM 50 镁合金表面制备涂层，研究添加黏土微粒对涂层显微组织、磨损和腐蚀行为的影响。采用铝基电解液制备 PEO 涂层，在电解液中添加 5 g/L 黏土颗粒，并与未添加的作对比。采用 SEM、EDS 和 XRD 对涂层的结构和成分进行表征。磨损测试采用球-盘式摩擦试验机，载荷为 2、5 和 10 N。在 0.5%(质量分数)NaCl 溶液中，采用极化和电化学阻抗(EIS)实验研究涂层的腐蚀行为。结果表明，在 5 和 10 N 载荷下，添加黏土颗粒使涂层的耐磨性下降。磨损表面的 SEM 结果显示，含有黏土颗粒的涂层其磨损机制为黏着磨损和磨粒磨损。含黏土涂层的磨损性能较差，与涂层的黏结强度较低、粗糙度较高有关。动电位极化实验表明，添加黏土颗粒使涂层的腐蚀速率略微降低。EIS 结果表明，含黏土涂层的耐腐蚀性归功于其较好的致密度。

关键词：磨损；腐蚀；黏土颗粒；等离子体电解氧化；镁合金

(Edited by Bing YANG)